Supporting Information

A dynamic passive thermoregulation fabric using metallic microparticles

Muluneh G. Abebe, Gilles Rosolen, Jeremy Odent, Jean-Marie Raquez, and Bjorn Maes*

Supplementary Notes

1 Generalized Lorenz-Mie extension using the far-field method

Calculating scattering Q_{sca}, extinction Q_{ext} and absorption Q_{abs} efficiency of a single microsphere using the far-field approximation:

$$\begin{aligned} Q_{sca} &= \frac{4k_m^2 e^{-2k_m x}}{(n_m^2+k_m^2)\left[1+(2k_m x-1)e^{2k_m x}\right]} \sum_{n=1}^{\infty}(2n+1)\left(|a_n|^2+|b_n|^2\right), \\ Q_{ext} &= \frac{4k_m^2 e^{-2k_m x}}{(n_m^2+k_m^2)\left[1+(2k_m x-1)e^{2k_m x}\right]} \mathrm{Re}\sum_{n=1}^{\infty}(2n+1)\left(a_n+b_n\right), \end{aligned} \tag{1}$$

and $Q_{abs} = Q_{ext} - Q_{sca}$. The Mie parameters are

$$\begin{aligned} a_n &= \frac{m\psi_n'(m_m x)\psi_n(mx) - m_m\psi_n(m_m x)\psi_n'(mx)}{m\xi_n'(m_m x)\psi_n(mx) - m_m\xi_n(m_m x)\psi_n'(mx)} \\ b_n &= \frac{m\psi_n(m_m x)\psi_n'(mx) - m_m\psi_n'(m_m x)\psi_n(mx)}{m\xi_n(m_m x)\psi_n'(mx) - m_m\xi_n'(m_m x)\psi_n(mx)} \end{aligned} \tag{2}$$

with $m = m_p/m_m$, where $m_p = n_p + ik_p$ and $m_m = n_m + ik_m$ are the particle and matrix complex refractive indices, respectively. $x = 2\pi r/\lambda$ is the size parameter, $\psi_n(\rho)$, $\xi_n(\rho)$, $\psi_n'(\rho)$, and $\xi_n'(\rho)$ are Riccati–Bessel functions and their derivatives with respect to the argument ρ. When both $k_m x << 1$ and $k_m << n_m$, the above equations will reduce to the conventional Lorenz-Mie form.[1–6]

2 RTE analysis

2.1 Refraction angle and surface reflection

In ray tracing the path length of photons within the medium changes with the entrance angle, thus, calculation of refraction angle θ_2 at the air-medium interface $(n_1, k_1\text{-}n_2, k_2)$ is handled using the generalized Snell's law:[7]

$$p\tan\theta_2 = n_1\tan^{-1}(\sin\theta_1), \tag{3}$$

where θ_1 is the incidence angle and

$$p = \frac{1}{2}\left[\sqrt{\left(n_2^2 - k_2^2 - n_1^2\sin^2\theta_1\right)^2 + 4n_2^2k_2^2} + \left(n_2^2 - k_2^2 - n_1^2\sin^2\theta_1\right)\right] \tag{4}$$

The surface reflectance is calculated using Fresnel's relations:[7]

$$\begin{aligned} R_\parallel &= \frac{\left(p - n_1\sin\theta_1\tan\theta_1\right)^2 + q^2}{\left(p + n_1\sin\theta_1\tan\theta_1\right)^2 + q^2}R_\perp \\ R_\perp &= \frac{\left(n_1\cos\theta_1 - p\right)^2 + q^2}{\left(n_1\cos\theta_1 + p\right)^2 + q^2}, \end{aligned} \tag{5}$$

where subscripts $\parallel$ and $\perp$ denotes parallel and perpendicular to the air-medium interface, respectively. While

$$q = \frac{1}{2}\left[\sqrt{\left(n_2^2 - k_2^2 - n_1^2\sin^2\theta_1\right)^2 + 4n_2^2k_2^2} - \left(n_2^2 - k_2^2 - n_1^2\sin^2\theta_1\right)\right] \tag{6}$$

and the surface specular reflectance $R^{12} = (R_\perp + R_\parallel)/2$.

2.2 Effective medium theory

For calculating the specular reflectance R^{12}, the medium complex refractive index is retrieved using the Maxwell-Garnett effective medium theory, as a function of the volume fraction of particles f_v, the dielectric function of the matrix ε_m and the particles ε_p:

$$\varepsilon_2 = \varepsilon_{\text{eff}} = \varepsilon_m\frac{2f_v\left(\varepsilon_p - \varepsilon_m\right) + \varepsilon_p + 2\varepsilon_m}{2\varepsilon_m + \varepsilon_p - f_v\left(\varepsilon_p - \varepsilon_m\right)}, \tag{7}$$

The refraction and absorption indices of the medium can be expressed in terms of the complex dielectric function, $\varepsilon_2 = \varepsilon_2' + i\varepsilon_2''$:

$$\begin{aligned} n_2^2 &= \tfrac{1}{2}\left(\varepsilon_2' + \sqrt{\varepsilon_2'^2 + \varepsilon_2''^2}\right) \\ k_2^2 &= \tfrac{1}{2}\left(-\varepsilon_2' + \sqrt{\varepsilon_2'^2 + \varepsilon_2''^2}\right) \end{aligned} \tag{8}$$

2.3 Collision-based forward Monte Carlo method

The phase function $\Phi(\Omega', \Omega)$ in the radiative transfer equation (RTE) is approximated using the Henyey-Greenstein phase function

$$\Phi_{HG}(\Theta) = \frac{1 - g^2}{\left(1 + g^2 - 2g\cos\Theta\right)^{3/2}}, \tag{9}$$

where g is the asymmetry factor and Θ is the angle between the direction of the ray before scattering (Ω') and after scattering (Ω).[7,8] In terms of Cartesian coordinate, $\Phi(\theta'\phi'; \theta, \phi)$, if the incident ray is in the direction of one of the axes, for example z, then the angular deviation can be expressed using only two angles, θ (polar) and ϕ (azimutal).[8]

The MC simulation consists of individually tracing the propagation of N_p photon bundles, also referred to as rays, which interact with the absorbing and scattering medium. A ray is

characterized by its position, wavelength, and direction during its propagation throughout the medium.[9]

Each new ray is launched at the upper boundary of the medium. It may be reflected back or enter the medium. If it enters the medium, possible scattering and absorption events will take place. Rays that hit the internal side of the interfaces are reflected or transmitted accordingly. If the ray is reflected back to the medium it will go through another process of possible absorption or scattering. On the other hand, if it is transmitted through the top boundary it will contribute to the reflectance. If it is transmitted through the bottom boundary, it contributes to transmittance.

3 Thermal model analysis

3.1 Analytical model

We consider thermal dissipation from the human body to the ambient as a one-dimensional steady-state heat transfer problem. Heat generated by the human body is lost by three different heat transfer processes (conduction, radiation, and convection), thus the equality between total heat dissipation with metabolic heat generation (Q_{gen}) indicates an overall thermal comfort.

In the air gap by assuming there is no natural convection, the total heat flux Q_{air} is constituted from conduction (between skin and textile) and radiation (between skin and fabric as well as between the skin and ambient):

$$\begin{aligned} Q_{air} &= Q_{cond,air} + Q_{rad,air} + Q_{rad,tran} \\ &= -k_{air}(T)\frac{dT}{dx} + \varepsilon_{s,t}\sigma\left(T_{skin}^4 - T_{in}^4\right) + \varepsilon_{s,a}\sigma\left(T_{skin}^4 - T_{amb}^4\right), \end{aligned} \tag{10}$$

where σ is the Stefan-Boltzmann constant, $k_{air}(T)$ is the thermal conductivity of the air in the gap, which depends on the local temperature $T(x)$, T_{skin} and T_{amb} are the skin and ambient temperatures, T_{in} is the fabric inner side temperature, and the effective emissivity calculated using surface to surface net-radiation method (see Figure S10):

$$\begin{aligned} \varepsilon_{s,t} &= \frac{1}{\varepsilon_s^{-1} + \varepsilon_t^{-1} - 1}, \\ \varepsilon_{s,a} &= \frac{1}{\varepsilon_s^{-1} + \varepsilon_{amb}^{-1} + \tau^{-1} - 2}, \end{aligned} \tag{11}$$

with skin ε_s, ambient ε_{amb}, and fabric ε_t emissivity and fabric transmittance τ. The total heat flux in the fabric is composed of heat conduction and radiation transmission from skin to the ambient:

$$\begin{aligned} Q_{textile} &= Q_{cond,tex} + Q_{rad,tran} \\ &= -k_{MMDF}(T)\frac{dT}{dx} + \varepsilon_{s,a}\sigma\left(T_{skin}^4 - T_{amb}^4\right), \end{aligned} \tag{12}$$

with $k_{MMDF}(T)$ the effective thermal conductivity of the fabric.

By considering an air flow in the ambient, the total heat flux from the outer fabric surface is constituted by convection and radiation (between fabric and ambient as well as between

the skin and ambient):

$$\begin{aligned} Q_{amb} &= Q_{conv} + Q_{rad,amb} + Q_{rad,tran} \\ &= h\left(T_{out} - T_{amb}\right) + \varepsilon_{t,a}\sigma\left(T_{out}^4 - T_{amb}^4\right) + \varepsilon_{s,a}\sigma\left(T_{skin}^4 - T_{amb}^4\right) \end{aligned} \tag{13}$$

with h a convective heat transfer coefficient, T_{out} is the fabric outer surface temperature, and

$$\varepsilon_{t,a} = \frac{1}{\varepsilon_t^{-1} + \varepsilon_{amb}^{-1} - 1}. \tag{14}$$

In light of the above analyses (see Eq. 10, 12, and 13) one must note that the absorbing/emitting semitransparent nature of the fabric is modeled by combining $Q_{rad,air}$, $Q_{rad,amb}$, and $Q_{rad,tran}$. This stems from the following points: $Q_{rad,tran}$ is the same in the air gap, inside the textile and in the ambient (in front of textile), therefore, this equality defines the transparent nature of the fabric. For example, if the fabric becomes opaque, then $Q_{rad,tran} = 0$.[10] On the other hand, $Q_{rad,air}$ and $Q_{rad,amb}$ defines the absorbing/emitting nature of the fabric. For example if the fabric becomes non-absorbing/non-emitting, then $Q_{rad,air} = Q_{rad,amb} = 0$.[11]

In steady-state case, heat fluxes are constant in the system, thus the temperature field can be determined using the energy equation.[12,13] Based on Figure S4a, for $0 \leq x \leq t_1$ (air gap thickness t_{air})

$$\frac{d}{dx}\left[-k_{air}(T)\frac{dT}{dx}\right] = 0, \tag{15}$$

and for $t_1 \leq x \leq t_2$ (fabric thickness t)

$$\frac{d}{dx}\left[-k_{eff}(T)\frac{dT}{dx}\right] = 0. \tag{16}$$

The boundary conditions for the above two second-order differential equations are the continuity of temperature on the skin-air gap and air gap-fabric interfaces, as well as continuity of heat flux on the air-fabric interface and the fabric-ambient interfaces ($T(0) = T_{skin}, T(t_1) = T_{in}, Q_{air}(t_1) = Q_{textile}(t_1)$, and $Q_{textile}(t_2) = Q_{amb}(t_2)$). Multiple integration of Eq. 15 and Eq. 16 using the boundary conditions gives

$$t_1 = -\frac{1}{C_1}\int_{T_{skin}}^{T_{in}} k_{air}(T)dT \tag{17}$$

and

$$t_2 = t_1 - \frac{1}{C_2}\int_{T_{in}}^{T_{out}} k_{MMDF}(T)dT, \tag{18}$$

where C_1 and C_2 are integration constants. The physical meaning of C_1 is conduction in the air gap ($Q_{cond,air}$) and C_2 is conduction in the fabric ($Q_{cond,tex}$).

Using the energy balance of total heat fluxes in each layer (Eq. 10, Eq. 12, and Eq. 13) with heat flux boundary conditions, we introduce three more equations:

$$\begin{aligned} Q_{gen} &= C_1 + \varepsilon_{s,a}\sigma\left(T_{skin}^4 - T_{amb}^4\right) + \varepsilon_{s,t}\sigma\left(T_{skin}^4 - T_{in}^4\right) \\ C_2 &= C_1 + \varepsilon_{s,t}\sigma\left(T_{skin}^4 - T_{in}^4\right) \\ C_2 &= h\left(T_{out} - T_{amb}\right) + \varepsilon_{t,a}\sigma\left(T_{out}^4 - T_{amb}^4\right). \end{aligned} \tag{19}$$

This leads to five equations with five unknowns ($T_{in}, T_{out}, T_{amb}, C_1$, and C_2), thus in order to find a solution we define a vector function $f(z)$ with variables $z \equiv \{T_{in}, T_{out}, T_{amb}, C_1, C_2\}^T$ and $f \equiv \{f_1, f_2, f_3, f_4, f_5\}^T$ with its elements defined by

$$\begin{aligned}
f_1 &\equiv C_1 t_1 + \int_{T_{skin}}^{T_{in}} k_{air}(T) dT, \\
f_2 &\equiv C_2(t_2 - t_1) + \int_{T_{in}}^{T_{out}} k_{MMDF}(T) dT, \\
f_3 &\equiv Q_{gen} - C_1 - \varepsilon_{s,a}\sigma\left(T_{skin}^4 - T_{amb}^4\right) - \varepsilon_{s,t}\sigma\left(T_{skin}^4 - T_{in}^4\right) \\
f_4 &\equiv C_1 - C_2 + \varepsilon_{s,t}\sigma\left(T_{skin}^4 - T_{in}^4\right) \\
f_5 &\equiv C_2 - h\left(T_{out} - T_{amb}\right) + \varepsilon_{t,a}\sigma\left(T_{out}^4 - T_{amb}^4\right).
\end{aligned} \tag{20}$$

Finally one needs to find the vector z that satisfies $f(z) \equiv 0$. The Newton-Raphson method can be used to solve the equations iteratively.[14]

3.2 Effective thermal conductivity coefficient

The effective thermal conductivity coefficient in the fabric layer is calculated using a model for dilute metal-dielectric particulate composites developed by Ordonez-Miranda et al.[15]

$$\frac{k_{MMDF}}{k_m} = \frac{k_p(1+2l) + 2\chi k_m + 2\left[k_p(1-l) - \chi k_m\right] f_v}{k_p(1+2l) + 2\gamma k_m - \left[k_p(1-l) - \chi k_m\right] f_v}, \tag{21}$$

with metal microsphere thermal conductivity $k_p = k_e + k_{ph}$ (where k_e and k_{ph} are electron and phonon thermal conductivity, respectively), χ the electron-phonon coupling factor, k_m the thermal conductivity of the matrix, f_v the volume fraction of microspheres, $l = Rk_{ph}/r$ (with r the radius and R the interfacial thermal resistance).[12,13,16]

3.2.1 Temperature dependent air thermal conductivity coefficient

The temperature dependent thermal conductivity of air is fitted using a fourth order polynomial of the form $a_4T^4 + a_3T^3 + a_2T^2 + a_1T + a_0$, where T is temperature (see Table 1).

Property	Unit	a_4	a_3	a_2	a_1	a_0
$k_{air}(T)$	W/mK	2.98×10^{-15}	5.19×10^{-12}	-2.54×10^{-8}	7.56×10^{-5}	0.0236

Table 1: Fitting polynomial for k_{air}.

3.3 Thermal circuit analogy

The total heat loss of the system Q_{dry} is balanced by the metabolic heat generation Q_{gen}, and takes the following form in terms of total effective heat transfer resistance R_{eff}:

$$\begin{aligned}
Q_{gen} &= h_{eff}(T_{skin} - T_{amb}) \\
&= \frac{1}{R_{eff}}(T_{skin} - T_{amb}).
\end{aligned} \tag{22}$$

We use the thermal circuit model shown in Figure S3b, and implement basic summing rules:

$$R_{eff} = \left(\frac{1}{R_{air} + R_{cond,tex} + R_{amb}} + \frac{1}{R_{rad,trans}} \right)^{-1} \tag{23}$$

with

$$R_{air} = \left(\frac{1}{R_{rad,air}} + \frac{1}{R_{cond,air}} \right)^{-1} \text{ and } R_{amb} = \left(\frac{1}{R_{rad,amb}} + \frac{1}{R_{conv}} \right)^{-1}. \tag{24}$$

Following Fourier's law for thermal conduction, the conductive thermal resistances through the air gap and the textile are

$$R_{cond,air} = \frac{t_{air}}{k_{air}} \text{ and } R_{cond,tex} = \frac{t}{k_{MMDF}}, \tag{25}$$

where t_{air} and t are air and textile thickness, k_{air} is thermal conductivity coefficient of air and k_{MMDF} is the effective thermal conductivity of the fabric. Following Newton's law of cooling, the convective thermal resistance of the ambient air is:

$$R_{conv} = \frac{1}{h}, \tag{26}$$

where h is the convective coefficient of air. For the radiative thermal resistances in the air gap and the ambient, we have

$$R_{rad,air} = \frac{1}{4\sigma \bar{T}^3_{skin,in}} \left(\frac{1}{\varepsilon_s} + \frac{1}{\varepsilon_t} - 1 \right) \text{ and } R_{rad,amb} = \frac{1}{4\sigma \bar{T}^3_{out,amb}} \left(\frac{1}{\varepsilon_t} + \frac{1}{\varepsilon_{amb}} - 1 \right) \tag{27}$$

where σ is the Stefan-Boltzmann constant, $\varepsilon_{s,t,amb}$ are the emissivities of the skin, textile, and ambient environment. Here we considered the following simplification for temperatures:[10] $T_1^4 - T_2^4 \approx (T_1^2 - T_2^2)(T_1 + T_2)(T_1 - T_2)$, and we assume

$$\overline{T}^2 = \left(\frac{T_1 + T_2}{2} \right)^2 \approx T_1 T_2, \tag{28}$$

so $T_1^4 - T_2^4 = 4\overline{T}^3 \Delta T$, where $\Delta T = T_1 - T_2$. For the thermal resistance for radiation transmitted between the skin and the ambient environment through the textile, we have

$$R_{rad,tran} = \frac{1}{4\sigma \bar{T}^3_{skin,amb}} \left(\frac{1}{\tau} \right) \tag{29}$$

where $\bar{T}_{skin,amb} = \frac{T_{skin} + T_{amb}}{2}$ and τ is the transmissivity of the textile.

Supplementary Figures

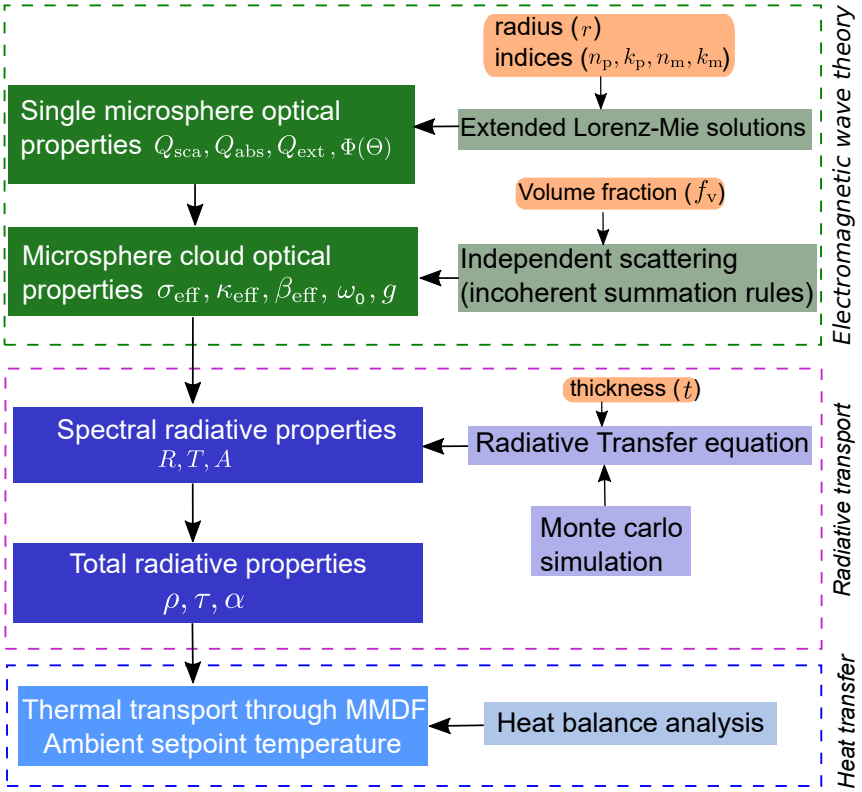

Figure S1. Modeling framework: First, we implement extended Lorenz-Mie solutions to calculate the optical properties of a single metallic microsphere, which includes scattering Q_{sca} (both forward Q^{f}_{sca} and backward Q^{b}_{sca}), extinction Q_{ext}, and absorption Q_{abs} efficiencies, and scattering phase function $\Phi(\Theta)$, where scattering angle Θ is the angle between the incident Ω' and scattered Ω directions. Second, using incoherent summation rule we calculate the effective radiative properties of a microsphere cloud uniformly dispersed in a polymer matrix (such as asymmetry factor g, scattering albedo ω_0, effective absorption κ_{eff}, scattering σ_{eff}, and extinction β_{eff} coefficients). Third, we solve radiative transfer equation using a collision-based forward Monte Carlo simulation to calculate spectral reflectance R, transmittance T, and absorptance A. Fourth, we calculate total reflectance ρ, transmittance τ, and absoptance α. Finally, we utilize a heat balance analysis to study thermal transport through the fabric, leading to the ambient setpoint temperature.

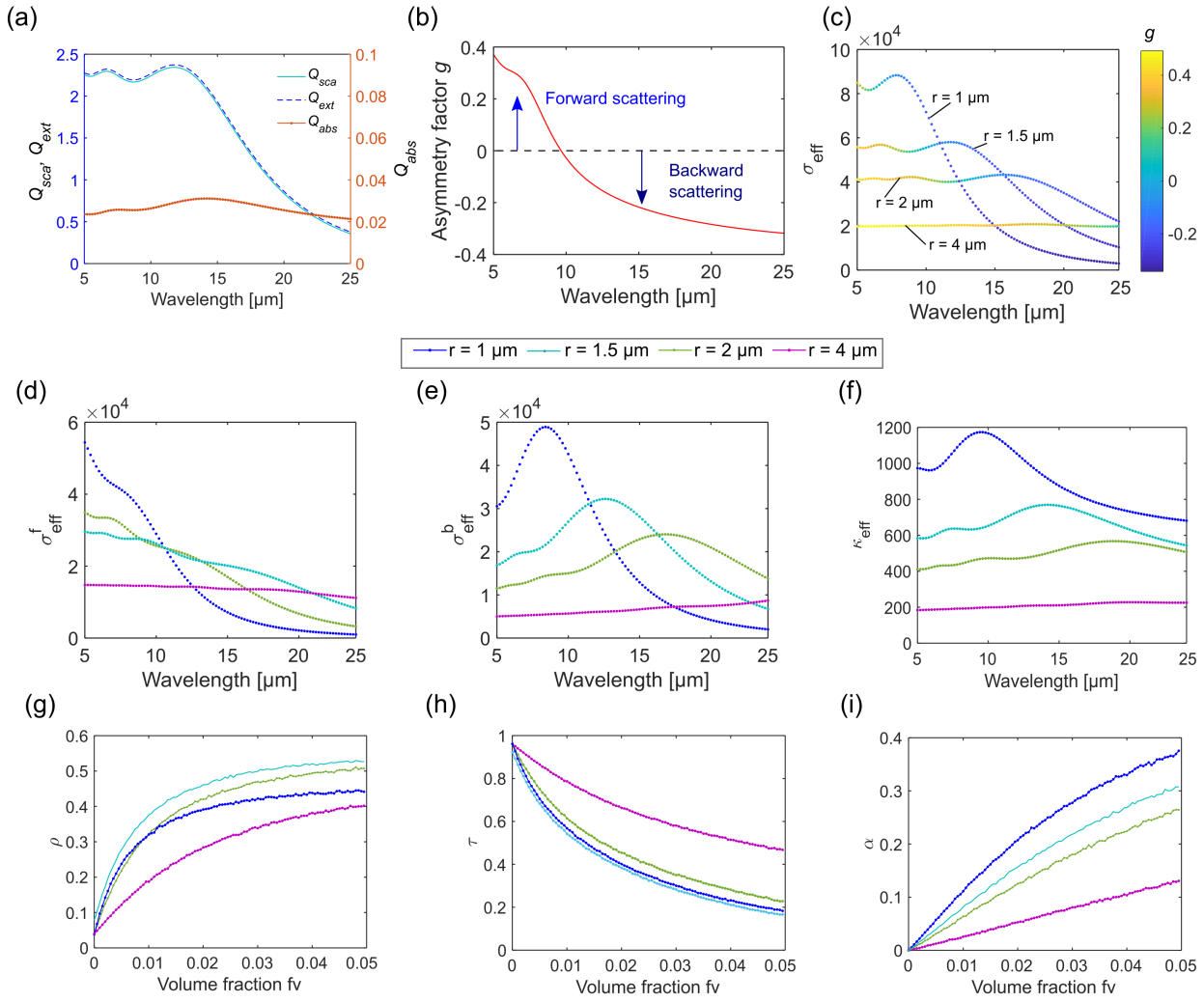

Figure S2. a) Q_{sca}, Q_{ext}, and Q_{abs}. b) g as a function of wavelength for r =1.5 μm Ag microsphere. c) Effective scattering coefficient (σ_{eff}) as a function of wavelength and g for r =1, 1.5, 2, and 4 μm Ag microspheres. d) Effective forward scattering coefficient σ^{f}_{eff}, e) backward scattering coefficient σ^{b}_{eff}, f) absorption coefficient σ_{eff}, g) total reflectance (ρ), h) transmittance (τ), and i) absorptance (α) for r =1, 1.5, 2, and 4 μm Ag microspheres.

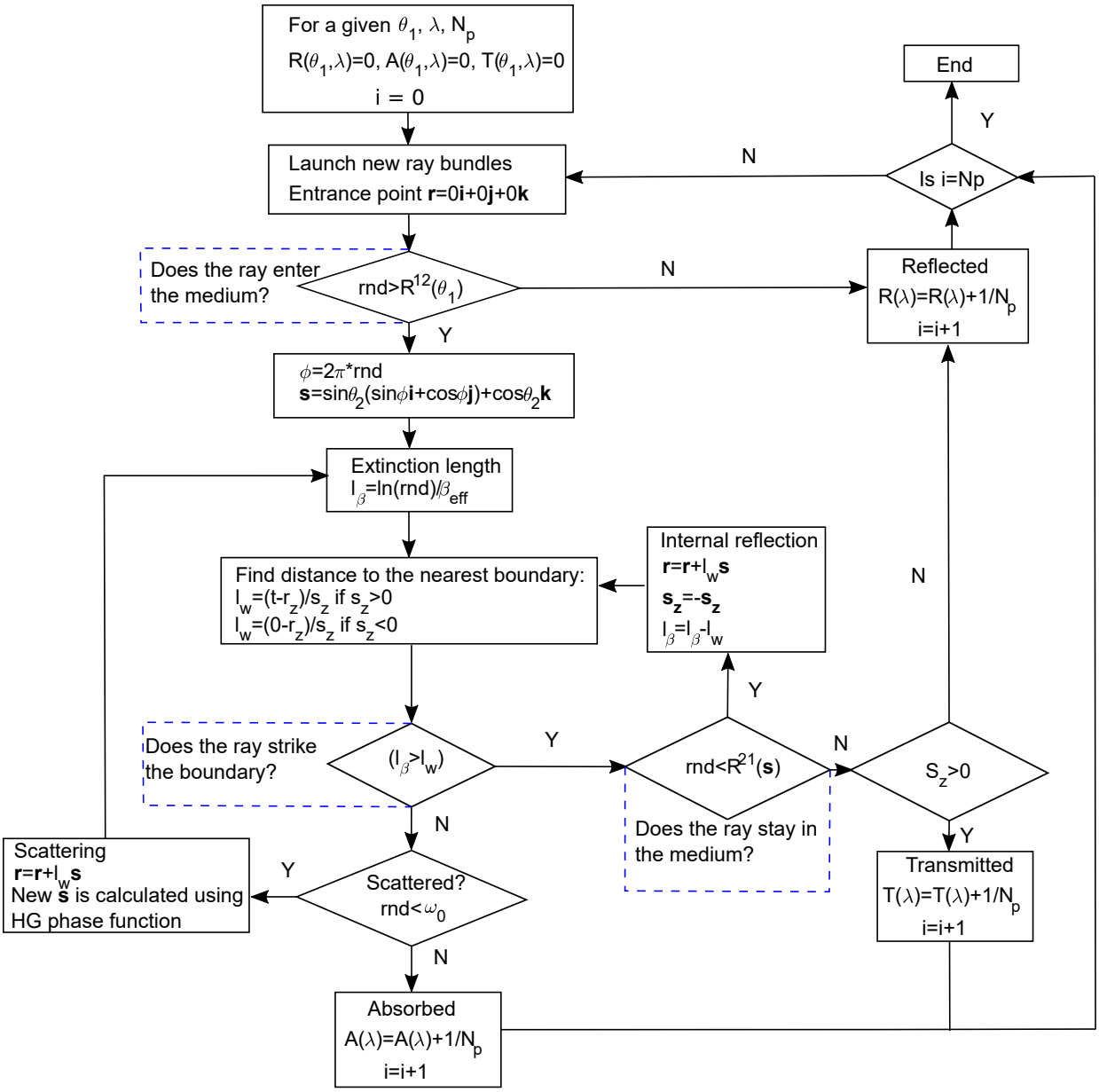

Figure S3. Flowchart for Monte Carlo solution of ray propagation in an absorbing and scattering semi-transparent medium. Where θ_1 and θ_2 are incident and entrance angles, λ wavelength, N_p number of rays, rnd is generated random number, R^{12} and R^{21} are boundary specular reflectances, $\mathbf{s} = s_x\mathbf{i} + s_y\mathbf{j} + s_z\mathbf{k}$ is the incoming direction, l_β is the extinction length, l_w is the distance to the nearest boundary, t is the thickness of fabric.

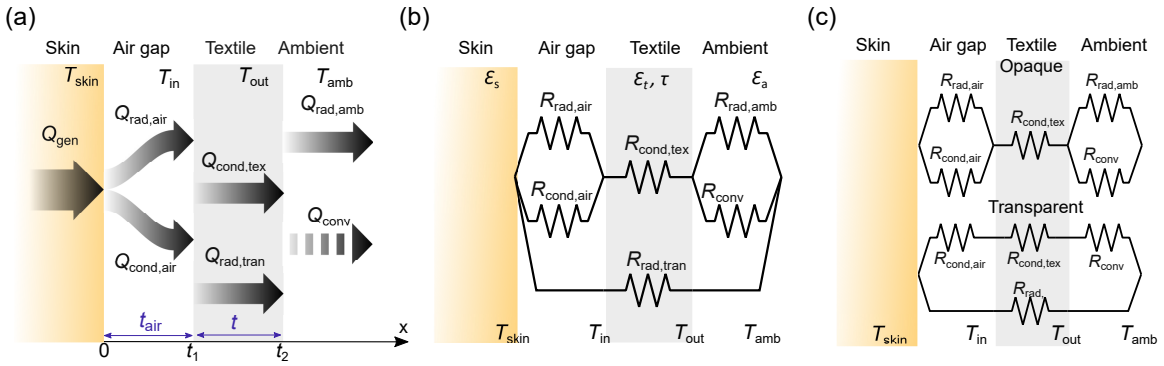

Figure S4. a) The main heat flow channels when the fabric covers skin, with an air gap in between. b) Thermal circuit analogy of semi-transparent fabric (MMDF). c) Thermal circuit analogy for opaque and transparent fabric.

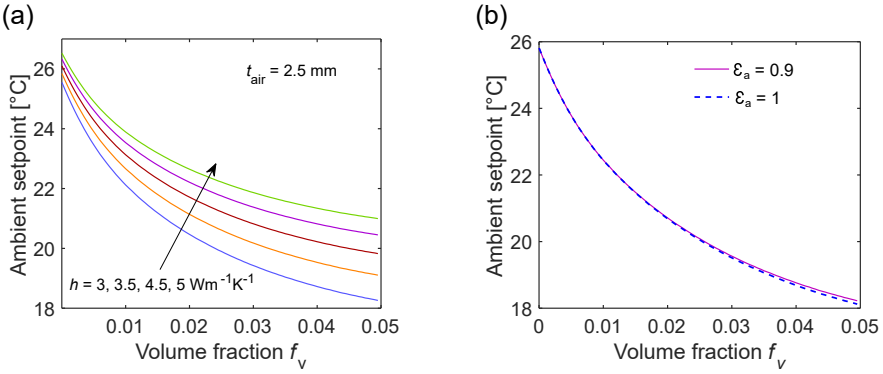

Figure S5. a) Ambient setpoint as a function of volume fraction for air gap thickness $t_{air} = 2.5$mm. The ambient air circulation effect is investigated, where the convective transfer coefficient h is varied. With increasing air circulation, the cooling functionality improves considerably, while negatively impacting the heating functionality. b) Ambient setpoint comparison between blackbody ($\varepsilon_a = 1$) and gray body ($\varepsilon_a = 0.9$) ambient. The upper bound setpoint temperature (cooling) is the same for both black and gray body ambient. In contrast, the lower bound setpoint temperature has a minimal change of about 0.1 °C. This is due to the net radiative exchange between fabric surface and ambient increases when the ambient emissivity decreases, thus, the heating functionality reduces.

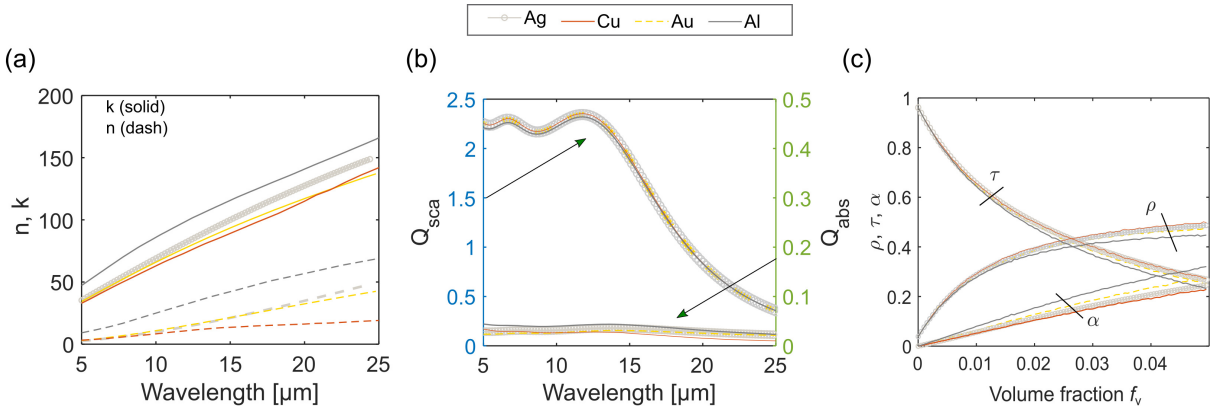

Figure S6. a) Refractive index (n) and extinction coefficient (k) of silver (Ag), copper (Cu), gold (Au), and aluminum (Al).[17] b) Q_{sca} and Q_{abs} of single metal microsphere with a size of $r = 1.5$ μm for Ag, Cu, Au, and Al. c) Calculated ρ, τ, and α as a function of f_v for a fabric thickness of $t = 150$ μm for Ag, Cu, Au, and Al microspheres.

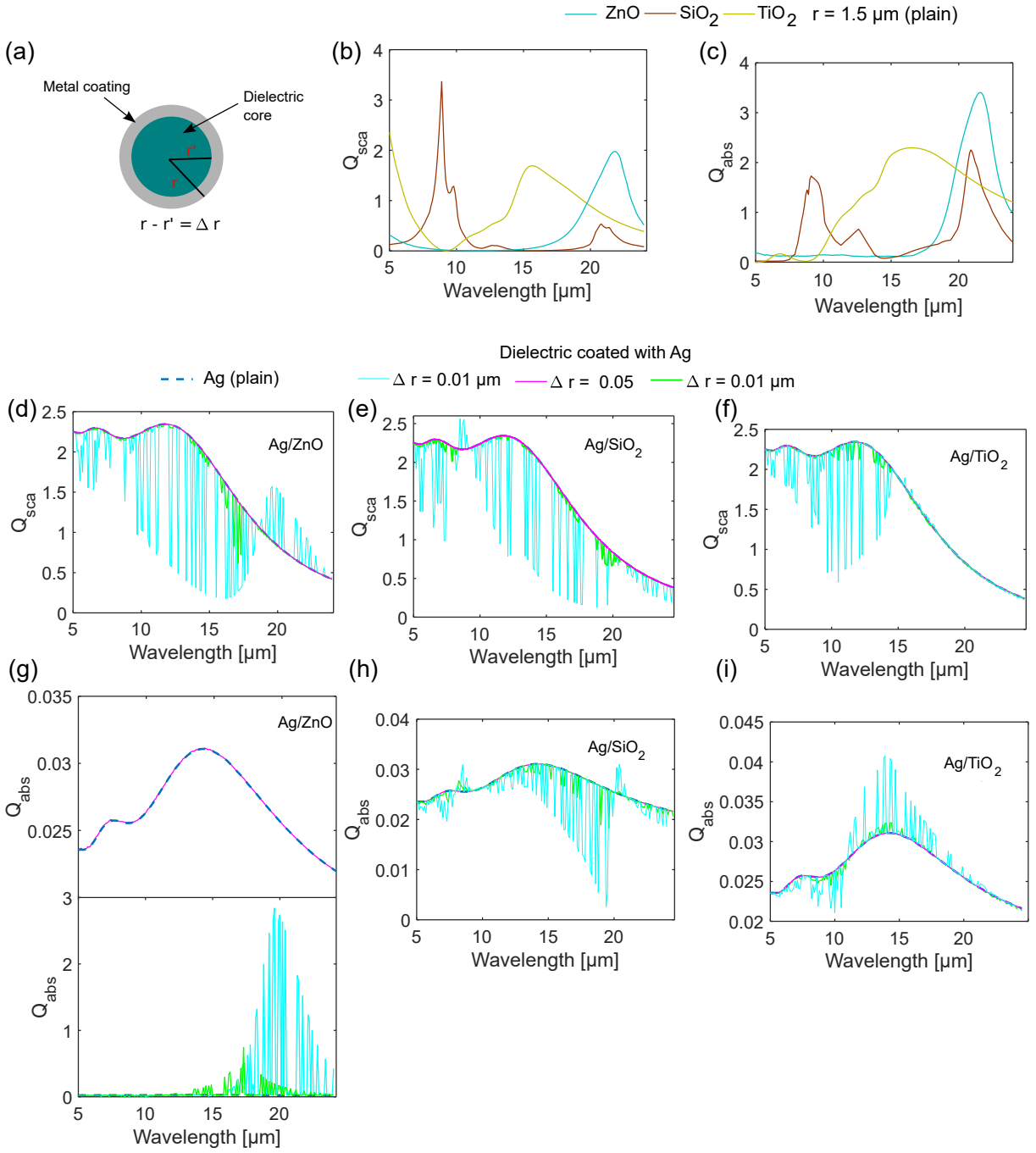

Figure S7. a) Schematic of core-shell microsphere with radius (r), core radius (r') and shell thickness Δr. b) Q_{sca} and c) Q_{abs} of single plain zinc-oxide (ZnO), silicon-dioxide (SiO_2), and titanium-dioxide (TiO_2) microsphere with a size of $r = 1.5$ μm. Q_{sca} comparison between plain Ag and coreshell d) Ag/ZnO, e) Ag/SiO_2, and f) Ag/TiO_2 with different coating thickness (Δr). A similar comparison for Q_{abs} is presented in g), h) and i) respectively. These results indicate that a Δr about 100 nm (solid pink line) and above gives the same radiative response as a plain metal microsphere of the same size ($r = 1.5$ μm).

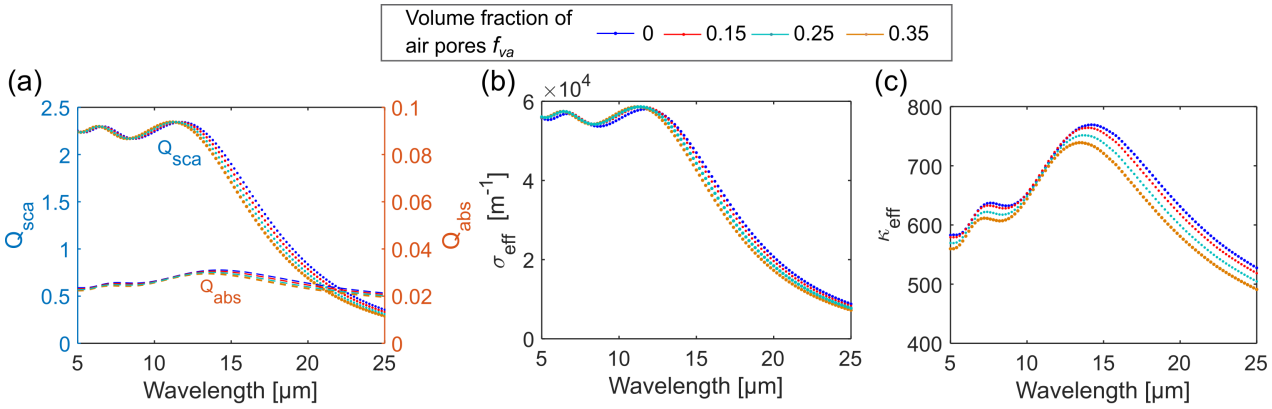

Figure S8. a) Q_{sca} and Q_{abs} of single metal microsphere with a size of $r = 1.5$ μm embedded in a nanoporous polymer medium for different air-pore volume fraction ($f_{va} = 0, 0.15, 0.25$, and 0.35). The corresponding particle cloud b) σ_{eff} and c) κ_{eff} with microsphere volume fraction of 0.05 and air-pore volume fraction ($f_{va} = 0, 0.15, 0.25$, and 0.35).

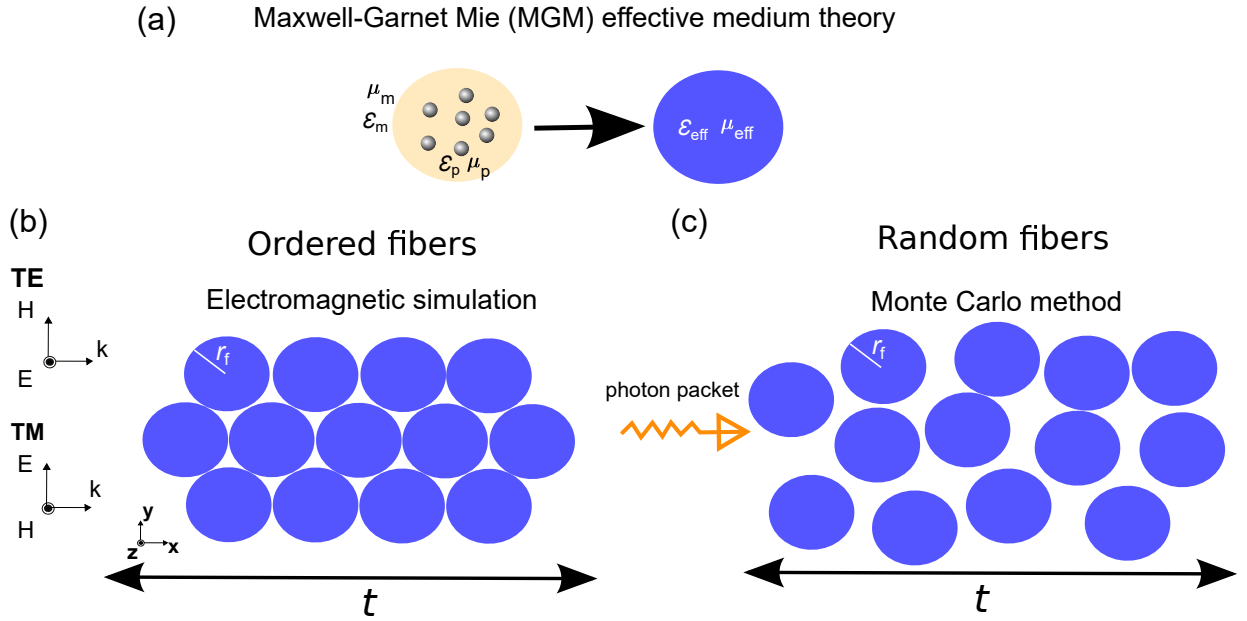

Figure S9. a) The effective complex index of refraction of the fiber is retrieved from $m_{eff} = n_{eff} + ik_{eff} = \sqrt{\epsilon_{eff}\mu_{eff}}$ using size dependent Maxwell-Garnet Mie (MGM) effective medium theory.[18,19] Where $\epsilon_{eff} = \epsilon_m\{1 + i\gamma[S(0) + S_1(\pi)]\}$ and $\mu_{eff} = 1 + i\gamma[S(0) - S_1(\pi)]$ are the effective electric permittivity and magnetic permeability of the fiber. Here, ϵ_m is the dielectric constant of the medium (polymer), $S(0)$ and $S_1(\pi)$ are the forward and backward scattering amplitudes calculated using the dielectric constant of Ag particle (ϵ_p). While, the factor $\gamma = 3f_v/2X^3$ with volume fraction of the particles f_v and size parameter in the medium $X = n_m k_o r$. Where, n_m is the refractive index of the medium, k_o is the wave vector in free space, and r is the radius of the particles. b) To calculate the IR radiative response (mainly reflectance R) of the ordered fibers design geometry, we use a finite-element-based Maxwell equations solver (COMSOL Multiphysics). The simulated geometry is constituted from ordered fibers with radius (r_f) in a hexagonal arrangement. The calculations are performed with incidence radiation in the x direction for transverse electric (TE) and transverse magnetic (TM) polarization. Floquet periodic boundary conditions are used on the top and bottom to represent an infinite repetition in the vertical direction, and the different diffraction orders are included using port conditions on the right and left sides. c) For the randomly distributed fiber configuration, we utilized collision-based Monte Carlo calculations to retrieve R, while each fiber's radiative property is acquired using Lorenz-Mie solutions for cylindrical geometry.

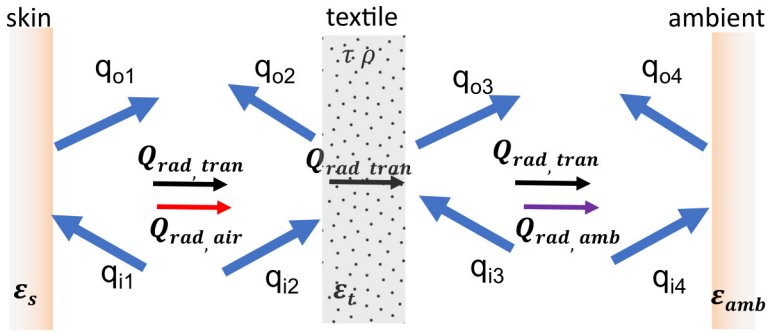

Figure S10. Schematics used for the net-radiation method to calculate radiative exchange between the skin, textile, and ambient. The detailed modeling reads as follows: For the transmitted part of the radiation, at the skin surface, $q_{i,1} + Q_{rad,tran} = q_{o,1}$ and $q_{o,1} = \varepsilon_1 \sigma T_{skin}^4 + (1 - \varepsilon_s)\, q_{i,1}$. At the ambient, $q_{i,4} = Q_{rad,tran} + q_{o,4}$ and $q_{o,4} = \varepsilon_{amb} \sigma T_{amb}^4 + (1 - \varepsilon_{amb})\, q_{i,4}$. At the textile surface, $q_{o,2} = q_{i,3}\tau + q_{i,2}\rho$ and $q_{o,3} = q_{i,2}\tau + q_{i,3}\rho$. Where τ and ρ are the total reflectance and transmittance of the fabric. The outward and inward radiative heat fluxes q_o and q_i are related as $q_{i,3} = q_{o,4}$, $q_{i,2} = q_{o,1}$, $q_{i,1} = q_{o,2}$, and $q_{i,4} = q_{o,3}$. These relations are solved for $Q_{rad,tran}$, which is the transmitted radiative flux through the textile from the skin to the ambient:

$$Q_{rad,tran} = \frac{\sigma \left(T_s^4 - T_{amb}^4\right)}{\frac{1}{\varepsilon_s} + \frac{1}{\varepsilon_{amb}} + \frac{1}{\tau} - 2}.$$

For radiative heat transfer between skin and textile inner surface, at the skin surface, $q_{i,1} + Q_{rad,air} = q_{o,1}$ and $q_{o,1} = \varepsilon_s \sigma T_{skin}^4 + (1 - \varepsilon_s)\, q_{i,1}$. At the textile inner surface, $q_{i,2} = Q_{rad,air} + q_{o,2}$ and $q_{o,2} = \varepsilon_t \sigma T_{in}^4 + (1 - \varepsilon_t)\, q_{i,2}$. Using, $q_{i,1} = q_{o,2}$ and $q_{i,2} = q_{o,1}$ and solving these relations for $Q_{rad,air}$, which is the radiative exchange between the skin and the inner side of the textile results in:

$$Q_{rad,air} = \frac{\sigma \left(T_{skin}^4 - T_{in}^4\right)}{\frac{1}{\varepsilon_s} + \frac{1}{\varepsilon_t} - 1}.$$

For radiative heat transfer between the textile outer surface and ambient, at the textile outer surface, $q_{i,3} + Q_{rad,amb} = q_{o,3}$ and $q_{o,3} = \varepsilon_t \sigma T_{out}^4 + (1 - \varepsilon_t)\, q_{i,3}$. At the ambient, $q_{i,4} = Q_{rad,amb} + q_{o,4}$ and $q_{o,4} = \varepsilon_{amb} \sigma T_{amb}^4 + (1 - \varepsilon_{amb})\, q_{i,4}$. By utilizing, $q_{i,3} = q_{o,4}$ and $q_{i,4} = q_{o,3}$ and solving these relations for $Q_{rad,amb}$ results in:

$$Q_{rad,amb} = \frac{\sigma \left(T_{out}^4 - T_{amb}^4\right)}{\frac{1}{\varepsilon_t} + \frac{1}{\varepsilon_{amb}} - 1}.$$

References

[1] W. Mundy, J. Roux, A. Smith, *JOSA* **1974**, *64*, 12 1593.

[2] G. Videen, W. Sun, *Applied optics* **2003**, *42*, 33 6724.

[3] I. W. Sudiarta, P. Chylek, *JOSA A* **2001**, *18*, 6 1275.

[4] Q. Fu, W. Sun, *Applied Optics* **2001**, *40*, 9 1354.

[5] J. Yin, L. Pilon, *JOSA A* **2006**, *23*, 11 2784.

[6] P. Yang, B.-C. Gao, W. J. Wiscombe, M. I. Mishchenko, S. E. Platnick, H.-L. Huang, B. A. Baum, Y. X. Hu, D. M. Winker, S.-C. Tsay, et al., *Applied optics* **2002**, *41*, 15 2740.

[7] M. F. Modest, *Radiative heat transfer*, Academic press, **2013**.

[8] J. R. Howell, M. P. Mengüç, K. Daun, R. Siegel, *Thermal radiation heat transfer*, CRC press, **2020**.

[9] F. Retailleau, V. Allheily, L. Merlat, J.-F. Henry, J. Randrianalisoa, *Journal of Quantitative Spectroscopy and Radiative Transfer* **2020**, 107300.

[10] P.-C. Hsu, C. Liu, A. Y. Song, Z. Zhang, Y. Peng, J. Xie, K. Liu, C.-L. Wu, P. B. Catrysse, L. Cai, et al., *Science advances* **2017**, *3*, 11 e1700895.

[11] M. G. Abebe, G. Rosolen, E. Khousakoun, J. Odent, J.-M. Raquez, S. Desprez, B. Maes, *Physical Review Applied* **2020**, *14*, 4 044030.

[12] C.-W. Nan, R. Birringer, D. R. Clarke, H. Gleiter, *Journal of Applied Physics* **1997**, *81*, 10 6692.

[13] D. Hasselman, L. F. Johnson, *Journal of composite materials* **1987**, *21*, 6 508.

[14] D. Ding, T. Tang, G. Song, A. McDonald, *Textile Research Journal* **2011**, *81*, 4 398.

[15] J. Ordonez-Miranda, R. Yang, J. Alvarado-Gil, *Journal of Applied Physics* **2012**, *111*, 4 044319.

[16] S. A. Faroughi, C. Huber, *Journal of Applied Physics* **2015**, *117*, 5 055104.

[17] M. A. Ordal, R. J. Bell, R. W. Alexander, L. L. Long, M. R. Querry, *Applied optics* **1985**, *24*, 24 4493.

[18] Y. Battie, A. Resano-Garcia, N. Chaoui, Y. Zhang, A. En Naciri, *The Journal of chemical physics* **2014**, *140*, 4 044705.

[19] R. G. Barrera, A. Garcıa-Valenzuela, *JOSA A* **2003**, *20*, 2 296.